Mineralogical Magazine, February 2016, Vol. 80(1), pp. 187–198

Phases in the Ni–Sb–As system which occur in the Bon Accord oxide body, Barberton greenstone belt, South Africa

M. Tredoux[1,*], F. Zaccarini[2], G. Garuti[2] and D. E. Miller[1]

[1] Department of Geology, University of the Free State, PO Box 339, Bloemfontein 9300, South Africa
[2] Department of Applied Geosciences and Geophysics, University of Leoben, Peter Tunner Str. 5, A-8700 Leoben, Austria

[*Received 7 October 2013; Accepted 10 March 2015; Associate Editor: W. Crichton*]

ABSTRACT

An oxide-silicate occurrence, containing >40 wt.% NiO whole rock and showing enrichment in the platinum-group elements and antimony, was investigated at high magnification. Many phases with grain sizes generally <100 μm were observed; electron microprobe analysis indicated that, although some of these are known minerals in Ni–Sb–As space (such as breithauptite and orcelite), most of them cluster around the following compositions: Ni_3Sb, $Ni_3(Sb,As)$, Ni_3As, $Ni_5(Sb,As)_2$, $Ni_7(Sb,As)_3$ and $Ni_{11}(Sb,As)_8$. Such phases have been observed in synthetic systems, but up to now not in nature. The data reported here therefore probably represent the compositions of new minerals.

Introduction

The Bon Accord oxide-silicate body was discovered about a century ago, during routine geological exploration in the north-western sector of the Barberton greenstone belt (BGB; see Fig. 1). It consisted of a single dense, dark-to-light green elliptical outcrop, with a sharp contact with the host rock (Trevor, 1920). Because of its unusually high NiO values (>35% whole rock; Trevor, 1920), the entire visible mass was removed, leaving a hole ~6 m^3 in size (de Waal, 1978). However, the material proved to be too refractory to smelt (Crosse, 1921, as reported by Partridge, 1944), and the ore was discarded as a disordered pile ~3 km from the original outcrop position (see Fig. 2), near the Sheba railway siding. None of the material was left *in situ*.

The origin and exact nature of the Bon Accord oxide are a highly controversial topic. The reader is referred to the following discussions: (1) de Waal (1978) who proposed that the Bon Accord oxide body represented an oxidized remnant of an Archaean iron meteorite; (2) Tredoux *et al.* (1989), who rejected the meteorite hypothesis of de Waal (1978) and suggested various possible terrestrial mechanisms for the generation of such a highly Ni-enriched composition in the absence of massive sulfide; (3) Wildau (2012) who favoured hydrothermal alteration of a magmatic spinel-olivine precursor; and (4) O'Driscoll *et al.* (2014), who proposed that it is a desulfurized NiS deposit (Kambalda type). These possibilities will not be elaborated on further in this paper, except to mention that the case in favour of a terrestrial origin for the Bon Accord oxide body has been strengthened by recent Cr isotopic data (Tredoux *et al.*, 2014): the εCr^{53} of the Bon Accord oxide, relative to a terrestrial standard, is 0 ± 0.01 epsilon units.

The mineralogy of the Bon Accord oxide

In the 1960s de Waal embarked on a thorough mineralogical study of the Bon Accord oxide ore, during which he discovered six new minerals (listed in Table 1) and confirmed the presence of trevorite which had previously been described by Walker (1923, as reported by Partridge, 1944) from alluvial material found in the vicinity. The current study does not seek to expand the work on major phases, and the reader is referred to Wildau (2012) and the various papers of de Waal and co-workers for details about their properties.

* E-mail: mtredoux@ufs.ac.za
DOI: 10.1180/minmag.2015.079.7.07

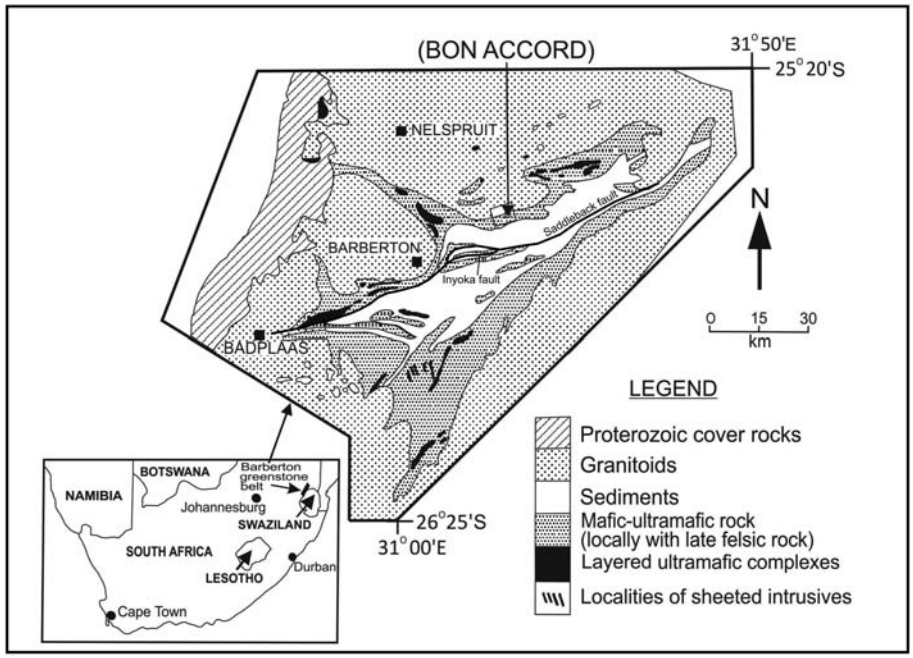

FIG. 1. The regional setting of the Barberton greenstone belt, and the position of the Bon Accord body. Adapted from Tredoux *et al*. (1989).

De Waal (1978) divided the body into five zones, from a dense, undeformed central region through concentric bands of increasing schistosity. Ideally all subsequent research should have been placed within this framework but near the end of the 1970s the ore pile mentioned in the introduction 'disappeared', and only a few hand specimens now are available for study. As a consequence, Tredoux *et al*. (1989) settled for a much simpler division into two groups only, as shown in Fig. 3: BAA (undeformed and dark green in colour; presumed on the basis of de Waal's (1978) descriptions to represent the core zone, or kernel, of the body) and BAB (lighter green and schistose; representing the surrounding rim). In cases of doubt based on optical properties, the subdivision was undertaken

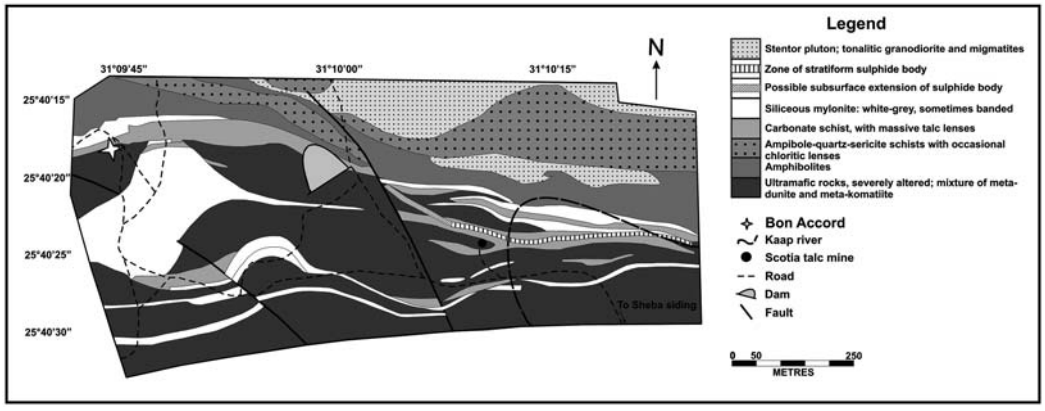

FIG. 2. The local geology of the area around the Bon Accord body. Adapted from Tredoux *et al.* (1989).

https://doi.org/10.1180/minmag.2015.079.7.07 Published online by Cambridge University Press

TABLE 1. Macroscopic Ni minerals from the Bon Accord deposit, after de Waal (1972, 1978, 1979), de Waal and Calk (1973) and Walker (1923). New Minerals first discovered and described from the Bon Accord deposit are shown in bold.

	Mineral name	Composition
Ni olivine	**Liebenbergite**	**Ni_2SiO_4**
Ni oxide	Bunsenite	NiO
Ni spinel	**Trevorite**	**$NiFe_2O_4$**
Ni-Co-Cr spinel	**Nichromite**	**$NiCr_2O_4$**
	Cochromite	**$CoCr_2O_4$**
Ni serpentine	Nepouite	$Ni_3Si_2O_5(OH)_4$
Ni talc	**Willemseite**	**$(Ni,Mg)_3Si_4O_{10}(OH)_2$**
Ni chlorite	**Nimite**	**$(Ni,Mg)_6Al_2Si_3O_{10}(OH)_8$**
Ni borate	**Bonaccordite**	**Ni_2FeBO_5**
Ni carbonate	Gaspeite	$(Ni,Mg)CO_3$

using geochemical indicators, specifically the platinum-group element (PGE) and Sb concentrations: the kernel is strongly enriched in these elements relative to the rim zone (Tredoux *et al*., 1989).

More recently, Wildau (2012) used petrological indicators, mainly microscopic deformation textures, and the composition of trevorite to arrange a set of twelve BA samples from the University of the Free State (UFS) archive in a more detailed order according to de Waal's (1978) criteria; her study included the following samples also used by Tredoux *et al*. (1989): BA-83.1 (classified as BAA by Tredoux *et al*. (1989), and considered by Wildau (2012) as the innermost one she examined, i.e. type I of de Waal (1978)), BA-84.1 (BAB, probably from de Waal's zone III (Wildau, 2012)) and BA-84.3 (BAB, probably zone V (Wildau, 2012)).

The geochemical features of the Bon Accord oxide body are very uncommon (Tredoux *et al*., 1989): High concentrations of Ni (>40 wt.% NiO, whole rock), Sb (>2000 ppm) and the PGE (>6000 ppb, slightly depleted in Os, Ir and Ru, relative to chondrite, in the kernel, and more strongly depleted in these elements in the rim zone) are the outstanding hallmarks of BAA. There is a virtual absence of S (<100 ppm whole rock; de Waal, 1978 and Wildau, 2012), especially in the kernel. It is important to note that pseudomorphed remnants of pre-existing massive sulfide have not been observed in any of the Bon Accord oxide samples studied by the current authors, nor reported by de Waal (1978, 1979), Tredoux *et al*. (1989) or Wildau (2012). It therefore seems as though low S was a primary characteristic of the material, especially of the core zone, although S clearly was added to the outer parts of the body later (O'Driscoll *et al*., 2014).

The dominant mineral in the BAA samples is trevorite, with the BAB samples being dominated by the silicates and carbonates (see Fig. 3). Wildau (2012) concluded that there are two generations of trevorite, and that the first of these formed early in the paragenesis by replacement of cochromite which, together with coarse-grained liebenbergite, formed the primary mineral assemblage. No Mg- or Fe-rich cores in the liebenbergite have been reported by de Waal and Calk (1973) or Wildau (2012), nor were any observed by the current authors. Hence, although the body undoubtedly has been affected by external factors, for example the intrusion of a Stentor granite batholith (de Waal, 1979) to the east (see Fig. 2), which most probably included chemical changes, the Ni enrichment of the silicates in the central part of the body appears to be a primary feature.

Although some of the host phases that account for the PGE have been identified (Zaccarini *et al*., 2014), and many of them also contain Sb and As, the PGMs are not abundant enough to account for all of the Sb and As enrichment. This paper reports research into other hosts of Sb and As, which have proved to be very elusive. In the course of the investigation, several Ni–Sb–As phases with chemistry not previously reported in natural material were encountered, and these will form the focus of this report. We also document the presence of native Ru in association with the Ni–Sb–As minerals, in support of the findings of Zaccarini *et al*., (2014).

https://doi.org/10.1180/minmag.2015.079.7.07 Published online by Cambridge University Press

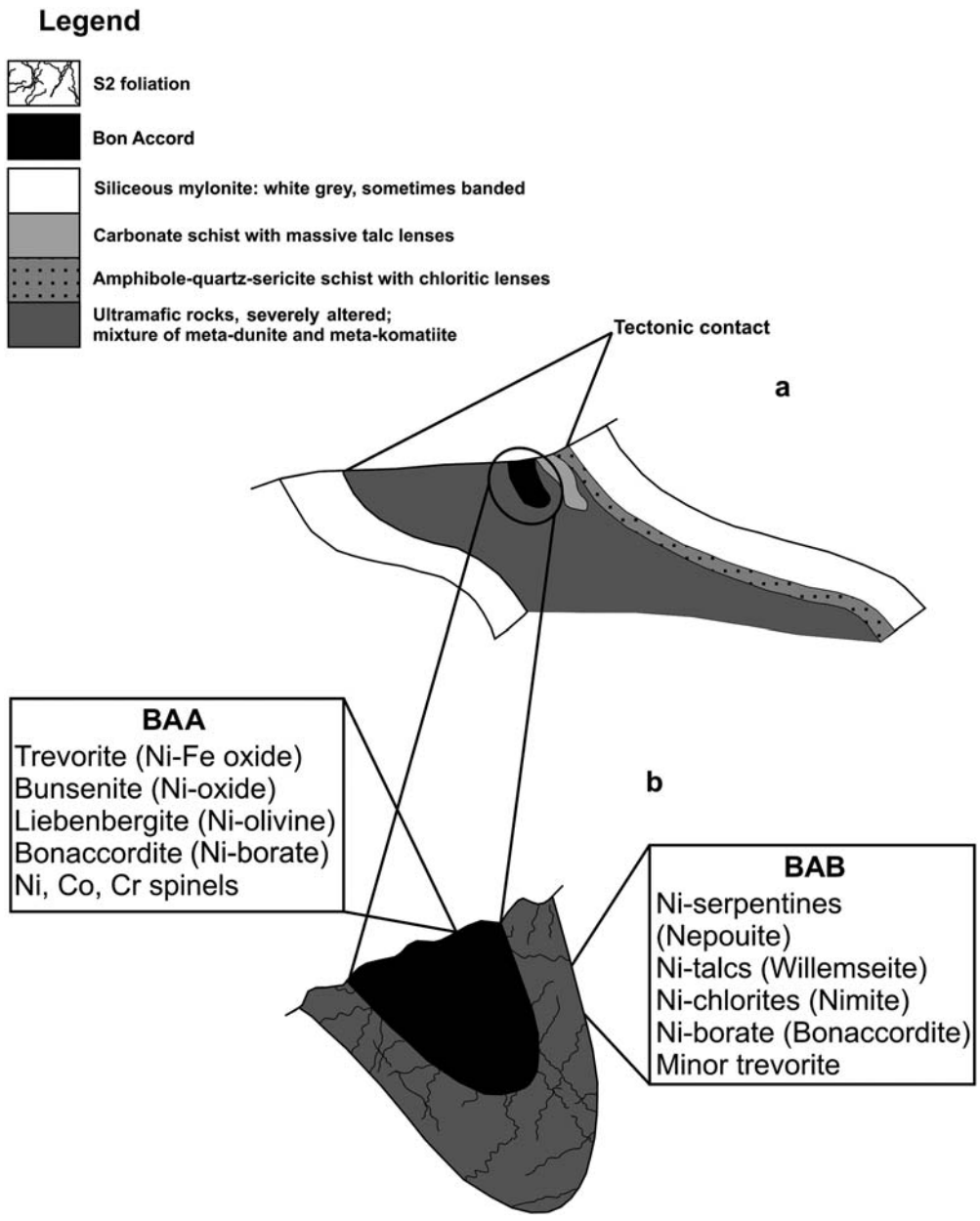

FIG. 3. A schematic representation of the distribution of Ni-rich minerals between the two major zones of the BA body. The dark-coloured area is BAA and the grey, lined area is BAB. Adapted from Tredoux *et al*. (1989).

Samples and analytical methodology

Two of the sets of thin and thick polished sections used for this investigation, called BA83-1 and BA87-1, were made from Bon Accord oxide samples collected in the 1980s by one of the authors (MT) from an abandoned core shed near the hole from which the ore body was removed. The third set, called BA-A, was prepared from a donation from a private collection. BA83-1

https://doi.org/10.1180/minmag.2015.079.7.07 Published online by Cambridge University Press

represents the massive centremost zone (BAA) as indicated in Fig. 3 (Wildau, 2012; see discussion above), and BA-A and BA87-1 are probably samples of the inner part of the schistose rim (BAB, probably de Waal's (1978) zone II or III).

The Ni-, Sb-, As- and PGE-bearing phases were located by scanning polished sections with a reflected light microscope at a magnification of 250–800× and also by backscattered electron (BSE) imaging, using Phillips XL 40 scanning electron microscopes (SEM) at the Universities of Cape Town (UCT; South Africa) and Modena a Reggio Emilia (UM; Italy), and a JEOL JXA-8200 electron microprobe at the Leoben University (LU; Austria). Typical analytical conditions were an accelerating voltage of 20 kV and a beam current of 10 nA. The phases of interest could be recognized easily, despite their small size (generally <15 μm) and very low modal abundance, because their high densities caused their backscattered component to be considerably higher than that of the matrix.

Subsequently, quantitative compositional data for Ni, Fe, Sb and As were obtained using the ARL-SEMQ wavelength dispersive electron microprobe (WD-EMP) at UM and the JEOL instrument at LU. The instruments were also operated at an accelerating voltage of 20 kV and a beam current of 10 nA, with a beam diameter of <1 μm. Synthetic NiAs and Sb_2S_3 were used as standards for the Ni, As and Sb, whereas Fe was calibrated on natural pyrite. The following X-ray lines were used in the analyses: Fe$K\alpha$, Ni$K\alpha$, As$L\alpha$ and Sb$L\alpha$.

Results

Phases in the Ni–Sb–As system

Because most of the grains studied were very small, generally <15 μm in diameter (or that being the longest dimension if the grain is not semi-spherical), the optical properties observed were limited to colour and isotropy, and were obtained for the biggest grains.

Under microscope observation in oil with tungsten-source illumination operated at ~3500 K, the Ni–Sb–As grains were yellowish, similar to millerite and heazlewoodite. They displayed very similar optical properties, despite different proportions of Ni–Sb–As (see below). Repeated observations made with different grains suggest that these minerals are either isotropic, or only slightly anisotropic, but due to the small grain size these observations might be misleading. Grain shapes varied from sharply defined six-sided crystals, often embayed, to rounded and oblate masses. They occurred associated with trevorite, liebenbergite and hydrated Ni-silicates (Fig. 4).

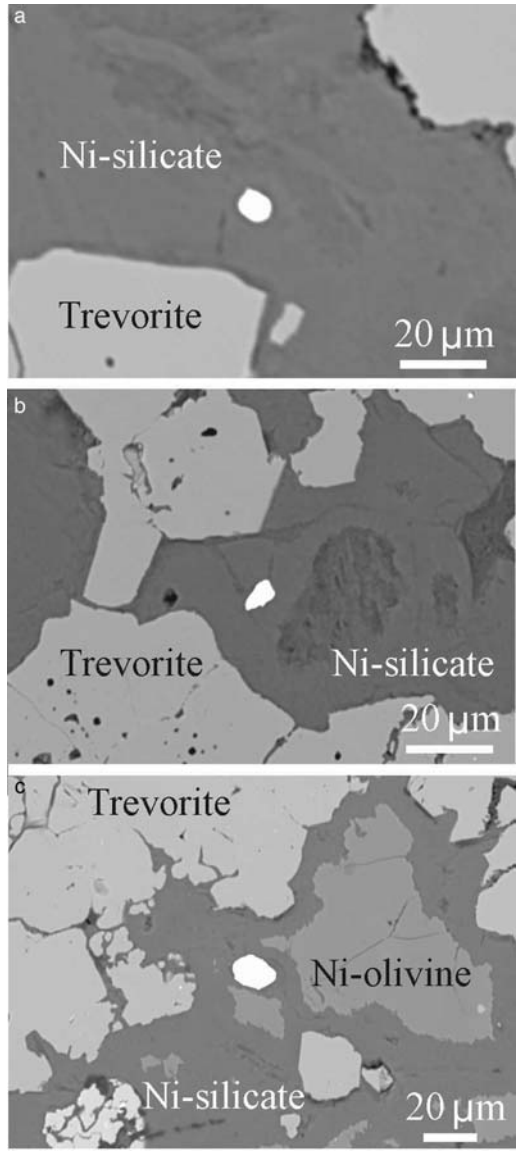

FIG. 4. Photomicrographs of the Bon Accord oxide body core (sample BA83.1), shown in backscattered electron mode. In all cases, the grains with high electron reflectance, ~10 μm in size, are examples of the phases reported on in this paper: (*a*) = Ni-rich orcelite, or Ni_7Sb_3; (*b*) = Ni_3Sb; (*c*) = $(NiFe)_3(SbAs)$.

https://doi.org/10.1180/minmag.2015.079.7.07 Published online by Cambridge University Press

TABLE 2. Representative compositions of Bon Accord minerals in the system Ni+(Fe)–Sb–As, with Sb>As (at.%).

		Ni	Fe	Sb	As	Total
Breithauptite						
Wt.%	BA-A 14 1	32.92	0.12	68.29	0.61	101.94
	BA-A 14 3	32.72	0.07	67.65	0.52	100.96
At%	BA-A 14 1	49.55	0.18	49.55	0.72	100
	BA-A 14 3	49.73	0.11	49.55	0.61	100
a.p.f.u.	BA-A 14 1	0.991	0.004	0.991	0.014	2
	BA-A 14 3	0.994	0.002	0.992	0.012	2
Ni_3Sb						
Wt.%	BA-A 1 1	59.19	0.08	41.50	0.34	101.11
	BA-A 2 1	59.52	0.07	41.54	0.40	101.51
	BA-A 3 1	58.21	1.30	41.00	0.50	101.01
	BA-A 5 1	58.06	0.11	40.77	0.30	99.24
	BA-A 8 1	58.72	0.06	41.74	0.36	100.88
	BA83-1 6 3	60.14	0.99	40.80	bdl	101.93
	BA83-1 7 1	59.34	0.42	40.62	bdl	100.38
	BA83-1 9 1	58.29	1.42	40.38	0.50	100.59
	BA83-1 10 2	59.19	0.08	41.50	0.34	100.81
	BA83-1 12 1	59.19	0.08	41.50	0.34	100.81
At.%	BA-A 1 1	74.41	0.10	25.15	0.34	100
	BA-A 2 1	74.47	0.09	25.05	0.39	100
	BA-A 3 1	73.01	1.71	24.79	0.49	100
	BA-A 5 1	74.38	0.15	25.17	0.30	100
	BA-A 8 1	74.15	0.08	25.41	0.36	100
	BA83-1 6 3	74.39	1.29	24.32		100
	BA83-1 7 1	74.77	0.54	24.67		100
	BA83-1 9 1	73.22	0.55	24.44	0.44	100
	BA83-1 10 2	73.96	1.45	24.50	0.09	100
	BA83-1 12 1	73.14	2.53	24.18	0.15	100
a.p.f.u.	BA-A 1 1	2.976	0.004	1.006	0.014	4
	BA-A 2 1	2.978	0.004	1.002	0.016	4
	BA-A 3 1	2.920	0.069	0.991	0.020	4
	BA-A 5 1	2.975	0.006	1.007	0.012	4
	BA-A 8 1	2.967	0.003	1.016	0.014	4
	BA83-1 6 3	2.976	0.051	0.973		4
	BA83-1 7 1	2.991	0.022	0.987		4
	BA83-1 9 1	2.928	0.074	0.978	0.020	4
	BA83-1 10 2	2.958	0.058	0.980	0.004	4
	BA83-1 12 1	2.926	0.101	0.967	0.006	4
Ni_7Sb_3						
Wt.%	BA83-1 3 2	53.79	0.42	46.68	bdl	100.89
	BA83-1 5 1	52.54	0.16	45.88	0.51	99.09
At%	BA83-1 3 2	70.11	0.57	29.32		100
	BA83-1 5 1	69.84	0.22	29.41	0.53	100
a.p.f.u.	BA83-1 3 2	7.101	0.057	2.932		10
	BA83-1 5 1	6.984	0.022	2.941	0.053	10
$Ni_{11}Sb_8$						
Wt.%	BA-A 3	39.03	1.07	60.94	bdl	101.04
At%	BA-A 3	56.14	1.61	42.25		100
a.p.f.u.	BA-A 3	10.665	0.307	8.028		19

'bdl' = below detection limit.

https://doi.org/10.1180/minmag.2015.079.7.07 Published online by Cambridge University Press

TABLE 3. Representative compositions of Bon Accord minerals in the system Ni+(Fe)–Sb–As, with As>Sb (at.%).

		Ni	Fe	Sb	As	Total
Ni_3As						
Wt.%	BA87-1 1 1	66.06	1.97	0.01	31.38	99.42
	BA87-1 2 1	66.31	1.38	0.09	31.43	99.21
	BA87-1 4 1	64.51	4.88	0.06	30.64	100.19
	BA87-1 8 1	62.69	6.72	0.01	29.80	99.22
	BA87-1 11 1	66.44	1.82	0.09	31.40	100.75
At.%	BA87-1 1 1	71.04	2.23	0.30	26.43	100
	BA87-1 2 1	71.45	1.56	0.46	26.53	100
	BA87-1 4 1	68.76	5.49	0.30	25.45	100
	BA87-1 8 1	67.07	7.55	0.41	24.97	100
	BA87-1 11 1	71.02	2.06	0.44	26.49	100
a.p.f.u.	BA87-1 1 1	2.844	0.087	0.012	1.057	4
	BA87-1 2 1	2.858	0.063	0.018	1.061	4
	BA87-1 4 1	2.750	0.220	0.012	1.018	4
	BA87-1 8 1	2.683	0.302	0.016	0.999	4
	BA87-1 11 1	2.841	0.082	0.017	1.060	4
$Ni_3(As,Sb)$						
Wt.%	BA83-1 1 1	63.49	0.89	20.40	15.80	100.51
	BA83-1 6 5	63.43	0.31	19.31	16.16	99.03
	BA83-1 7 2	63.43	0.52	18.90	16.67	99.52
	BA83-1 10 1	63.40	1.13	19.91	15.84	100.69
	BA83-1 12 4	62.88	1.07	21.05	14.96	99.96
	BA83-1 13 1	62.66	1.80	20.60	15.48	100.54
At.%	BA83-1 1 1	73.31	1.04	11.35	14.30	100
	BA83-1 6 5	74.07	0.38	10.77	14.78	100
	BA83-1 7 2	73.63	0.63	10.58	15.16	100
	BA83-1 10 1	73.34	1.37	11.03	14.26	100
	BA83-1 12 4	73.23	1.31	11.82	13.64	100
	BA83-1 13 1	72.35	2.19	11.46	14.00	100
a.p.f.u.	BA83-1 1 1	2.932	0.042	0.454	0.572	4
	BA83-1 6 5	2.963	0.015	0.431	0.591	4
	BA83-1 7 2	2.945	0.025	0.424	0.606	4
	BA83-1 10 1	2.934	0.054	0.441	0.571	4
	BA83-1 12 4	2.929	0.052	0.473	0.546	4
	BA83-1 13 1	2.917	0.072	0.494	0.517	4
$Ni_5(As,Sb)_2$						
Wt.%	BA-A 6 2	61.63	0.39	18.49	19.68	100.18
	BA-A 15 2	60.58	0.18	20.01	19.05	99.82
	BA-A 22B 1	61.57	0.25	19.74	19.33	101.11
	BA-A 29 3	62.47	0.29	19.35	19.31	101.41
	BA83-1 4 1	59.01	1.21	21.79	16.56	98.58
At.%	BA-A 6 2	71.35	0.47	10.32	17.86	100
	BA-A 15 2	70.98	0.22	11.30	17.50	100
	BA-A 23 1	71.03	0.44	11.74	16.79	100
	BA-A 29 3	71.63	0.52	10.70	17.35	100
	BA83-1 4 1	70.45	1.52	12.54	15.49	100
a.p.f.u.	BA-A 6 2	4.995	0.033	0.722	1.250	7
	BA-A 15 2	4.969	0.015	0.791	1.225	7
	BA-A 23 1	4.972	0.031	0.822	1.175	7
	BA-A 29 3	5.014	0.022	0.749	1.215	7
	BA83-1 4 1	4.932	0.106	0.878	1.084	7
$Ni_7(As,Sb)_3$ (or Sb-rich orcelite?)						

(continued)

https://doi.org/10.1180/minmag.2015.079.7.07 Published online by Cambridge University Press

TABLE 3. (*contd*.)

		Ni	Fe	Sb	As	Total
Wt.%	BA-A 6 1	59.23	0.34	18.11	21.86	99.54
	BA-A 26B 2	58.99	0.19	19.81	18.69	99.91
	BA83-1 8 1	58.31	1.21	22.59	17.33	99.44
At.%	BA-A 6 1	69.32	0.41	10.22	20.05	100
	BA-A 26B 2	70.75	0.23	11.46	17.56	100
	BA83-1 8 1	69.38	1.51	12.96	16.15	100
a.p.f.u.	BA-A 6 1	6.932	0.041	1.022	2.005	10
	BA-A 26B 2	7.075	0.023	1.146	1.756	10
	BA83-1 8 1	6.930	0.015	1.296	1.615	10
Ni_7As_3 (or orcelite?)						
Wt.%	BA87-1 1 1	65.96	1.97	0.58	31.33	99.84
	BA87-1 2 1	65.95	1.82	0.83	31.40	99.99
	BA87-1 11 1	66.34	1.38	0.89	31.45	100.06
At.%	BA87-1 1 1	71.04	2.23	0.30	26.43	100
	BA87-1 2 1	71.02	2.06	0.43	26.49	100
	BA87-1 11 1	71.45	1.56	0.46	26.53	100
a.p.f.u.	BA87-1 1 1	7.104	0.223	0.030	2.643	10
	BA87-1 2 1	7.102	0.206	0.043	2.649	10
	BA87-1 11 1	7.145	0.156	0.046	2.653	10

A selection of the 131 electron microprobe analyses is presented in Table 2 (for the Sb-rich phases) and Table 3 (for phases in which As is dominant). [A complete list of compositions has been deposited with the Principal Editor of *Mineralogical Magazine* and is available from www.minersoc.org/pages/e_journals/dep_mat_mm.html]. Apart from breithauptite (ideally NiSb), and orcelite ($Ni_{5-x}As_2$; confirmed by Bindi *et al*., 2014), seven other Ni–Sb–As phases have been identified. They are characterized by the following stoichiometries: Ni_3Sb, Ni_7Sb_3, $Ni_{11}Sb_8$, $Ni_3(As,Sb)$, $Ni_5(As,Sb)_2$, $Ni_7(As,Sb)_3$ and $Ni_{11}(As,Sb)_8$. Nickel is by far the most abundant element (generally between 70–75 at.% Ni, although a few grains with Ni as low as 50 at.% were observed), followed by Sb and As which are both very variable with ranges of 0–25 at%. Fe is generally ~1 at.% Fe or less, although some grains with Fe up to 5 at.% were observed. In general, the higher Fe concentrations occurred in phases in which As is very dominant over Sb.

Platinum-group minerals

Three of the Ni–Sb–As grains were associated with a single small (<2 μm diameter) rounded phase embedded along one of their crystal boundaries (see for example Fig. 5). These grains were identified as a different phase by much higher levels of electron backscattering from their surfaces. According to the qualitative energy-dispersive X-ray spectroscopy analyses, the three small bright grains were all native ruthenium. One grain of Ru occurred in contact with a grain characterized by the stoichiometry Ni_3Sb, included in trevorite (Fig. 5*a*). The other two grains of Ru were found associated with polyphase grains composed of a compound with the stoichiometry $Ni_7(As,Sb)_3$ inside hydrous Ni-silicate which occur with trevorite and Cl-rich apatite (Figs 5*b*,*c*). Although no other PGMs were observed in this study, Zaccarini *et al*. (2014) report a number of Pt ± Pd and Au minerals found in the <53 μm fraction of crushed Bon Accord material.

Discussion and concluding remarks

From the 37 compositions presented in Tables 2 and 3, it is clear that the data can be grouped into nine sets that are distinct and internally coherent, as evidenced by low coefficients of variation for the groups, if the elements are arranged as (Ni + Fe) and (Sb + As), as shown in Table 4. The groups reduce to the following ideal stoichiometries: with Sb > As (Table 2): (i) three of the analyses are of breithauptite; (ii) 26 of the analyses conform to

https://doi.org/10.1180/minmag.2015.079.7.07 Published online by Cambridge University Press

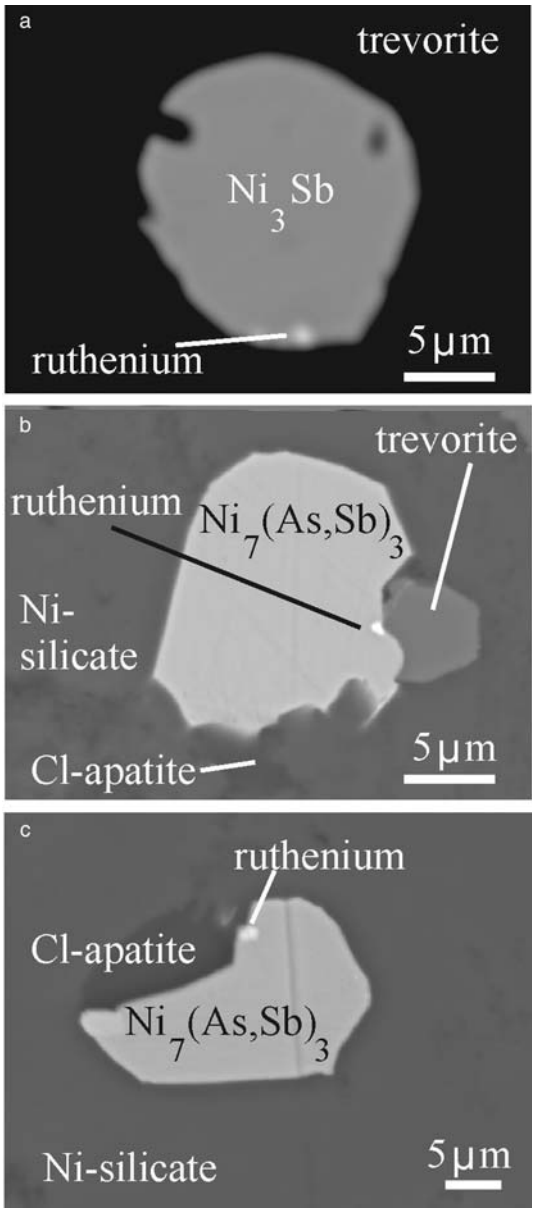

FIG. 5. High magnification photomicrographs of three of the (Ni + Fe)–Sb–As phases, each with a small (~1 µm) grain of native Ru attached to the edge.

Ni_3Sb; (iii) three analyses conform to Ni_7Sb_3; and (iv) one analysis conforms to $Ni_{11}Sb_8$. When the at.% of As is higher than Sb (Table 3), the following ideal stoichiometries have been calculated: (i) ten of the analyses conform to the formula Ni_3As; (ii) 15 of the analyses conform to $Ni_3(As,Sb)$; (iii) 27 of the analyses conform to $Ni_5(As,Sb)_2$; (iv) seven analyses conform to $Ni_7(As,Sb)_3$; and (v) three of the analyses conform to orcelite. Orcelite, breithauptite and $Ni_{11}Sb_8$ have also been reported by O'Driscoll *et al*. (2014).

According to their compositions and the ternary diagram shown in Fig. 6, seven of these phase compositions do not appear in any of the various listings of approved minerals, including the International Mineralogical Association list, as updated in August 2013 (see www.ima-mineralogy.org/Minlist.htm). Pre-1920 there was a 'mineral' with the supposed composition of Ni_3Sb, called dienerite, of which a single example was reported in 1892 from Radstadt, near Salzburg in Austria. This claim was discredited recently, as the real composition of the only example turned out to be $NiSb_3$, which is nickel-skutterudite, thus indicating that a typographical error was made in the original report of the composition (Bayliss, 2001). The group of analyses that approach the stoichiometry $Ni_7(As,Sb)_3$ are Sb-rich orcelite (Bindi *et al*., 2014); to the best of our knowledge, this is the first report of orcelite enriched in Sb. The $Ni_{11}Sb_8$ compound probably represents the Sb analogue of the mineral maucherite ($Ni_{11}As_8$), which has been identified tentatively in the Bon Accord oxide body by Wildau (2012) and O'Driscoll *et al*. (2014).

The Sb endmembers of the three Sb-rich phases, Ni_3Sb, Ni_7Sb_3 and Ni_5Sb_2, have been described by Raghavan (2004) and Okamoto (2009) in experimental studies of Ni–Fe–Sb alloys, as shown in Fig. 7. NiSb, Ni_3Sb and Ni_7Sb_3 are stable over a wide temperature range, but Ni_5Sb_2 only occurs at temperatures in excess of 600°C. This observation may imply that the alteration of the Bon Accord oxide body, and in particular the Ni enrichment which led to the formation of these phases, was caused by high-temperature fluids.

Raghavan (2004) assigned the following crystal structures to the Sb phase endmembers: Ni_3Sb as orthorhombic, with a β Cu-Ti type lattice; low temperature Ni_7Sb_3 as tetragonal; and the high temperature Ni_5Sb_2 as monoclinic. As 33 of the analysed grains in the Bon Accord oxide body have the same compositions of those reported by Raghavan (2004) and Okamoto (2009), they may represent the natural equivalent of the synthetic phases. However, their small sizes make it very difficult to obtain X-ray diffraction data to confirm this assumption. Research is currently underway to try to determine the physical properties of the phases. We tentatively suggest, based on their chemical composition only, that the following seven new Ni-

https://doi.org/10.1180/minmag.2015.079.7.07 Published online by Cambridge University Press

TABLE 4. A summary of all 95 compositions (at.%) of the (Ni + Fe)–Sb–As phases in the Bon Accord oxide body, with As and Sb considered as sharing the same lattice position. For phases with ≥5 analyses, the standard deviation and coefficient of variation (CoV) around the mean are given.

		Ni+Fe	As+Sb	*N*
Sb dominant (see Table 2 for typical analyses)				
Breithauptite	Mean (at.%)	49.69	50.31	3
Ni_3Sb	Mean (at.%)	75.21	24.79	26
	Std dev. (at.%)	0.53	0.53	
	CoV (%)	0.70	2.13	
Ni_7Sb_3	Mean (at.%)	70.49	29.74	3
$Ni_{11}Sb_8$	Single analysis only – see Table 2			
As dominant (see Table 3 for typical analyses)				
Ni_3As	Mean (at.%)	74.07	25.93	10
	Std dev. (at.%)	0.73	0.73	
	CoV (%)	0.98	2.80	
$Ni_3(As,Sb)$	Mean (at.%)	74.48	25.52	15
	Std dev. (at.%)	0.17	0.17	
	CoV (%)	0.22	0.65	
$Ni_5(As,Sb)_2$	Mean (at.%)	71.95	28.03	27
	Std dev. (at.%)	0.28	0.28	
	CoV (%)	0.39	0.99	
$Ni_7(As,Sb)_3$	Mean (at.%)	70.26	29.11	7
(or Sb-rich orcelite?)	Std dev. (at.%)	0.63	0.63	
	CoV (%)	0.90	2.12	
Ni_7As_3 (or orcelite?)	Mean (at.%)	70.49	29.51	3

N = number of analyses.

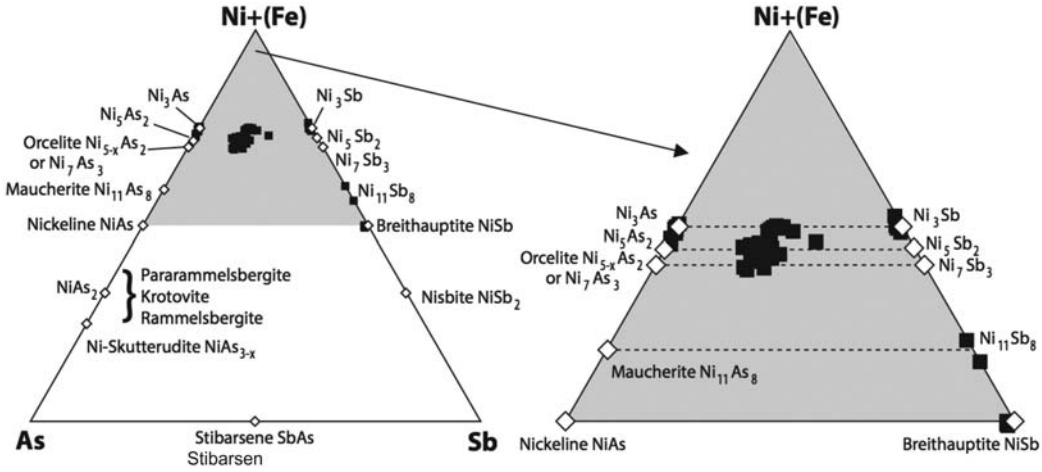

FIG. 6. Compositional fields of the new phases in the (Ni + Fe)–Sb–As ternary diagram. The open diamonds indicate ideal compositions, and the solid squares are 95 of the 131 data points from this study.

rich minerals have been found in the Bon Accord oxide body: Ni_3Sb, Ni_7Sb_3, $Ni_{11}Sb_8$, $Ni_3(As,Sb)$, $Ni_5(As,Sb)_2$, $Ni_7(As,Sb)_3$ and Ni_5As_2.

Regardless of the high PGE concentration in whole rock compositions of the Bon Accord oxide body (Tredoux *et al.*, 1989), during the present

https://doi.org/10.1180/minmag.2015.079.7.07 Published online by Cambridge University Press

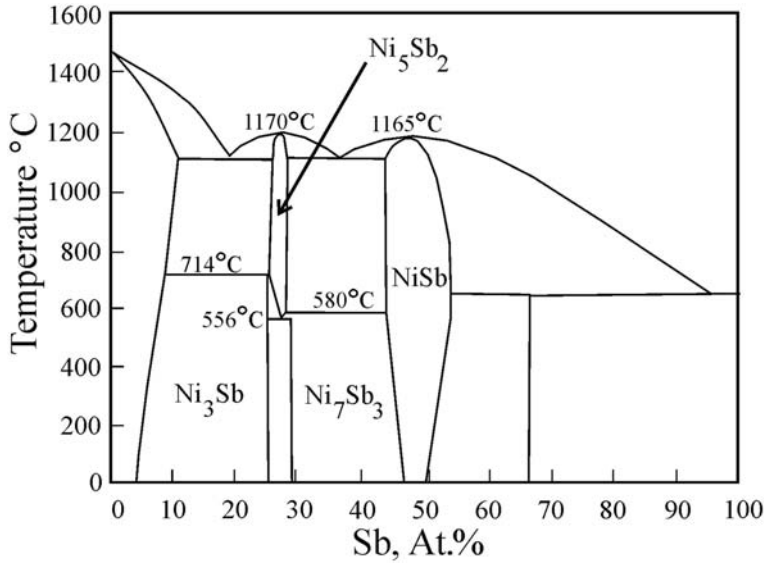

FIG. 7. The phase relations in the Fe–Ni–Sb system, as compiled by Okamoto (2004).

investigation only three small grains of native Ru were found. As no PGE nuggets were reported by de Waal (1972, 1978, 1979) and de Waal and Calk (1973), and none have been observed in the hand specimens of the current collection at the University of the Free State, it would appear that the high PGE concentrations reported by Tredoux *et al*. (1989) are caused either by rare µm-sized PGMs, or solid solution of the PGE in the major minerals, or the presence of sub-µm size nano phases of the type recently reported by Helmy *et al*. (2013). Alternatively, the PGE may occur as unconventional PGM, such as carbonates, oxides and/or hydroxides, that cannot readily be distinguished by optical and electron microscopy.

Acknowledgements

Tom Molyneux is thanked for his continued support of our research on the BA body, and for contributing to our collection of samples from his own. Mr Andries Felix is thanked for the drafting of Figs 1 and 2 and Ms Bianca Kennedy for Figs 3 and 6. The authors express gratitude to their home institutions for financial support, and in addition MT thanks the Inkaba ye Africa programme. The University Centre for Applied Geosciences (UCAG) of Leoben University is thanked for access to the E.F. Stumpfl Electron Microprobe Laboratory.

References

Bayliss, P. (2001) Dienerite – a mystification. *Mineralogical Magazine*, **65**, 685–687.

Bindi, L., Tredoux, M., Zaccarini, F., Miller, D.E. and Garuti, G. (2014) Non-stoichiometric nickel arsenides in nature: The structure of orcelite, $Ni_{5-x}As_2$ (x = 0.25), from the Bon Accord oxide body, South Africa. *Journal of Alloys and Compounds*, **601**, 175–178.

Crosse, A.F. (1921) A rich nickel ore. *Journal of the Chemical Society of South Africa*, **21**, 126.

De Waal, S.A. (1972) Nickel minerals from Barberton, South Africa: V: Trevorite, redescribed. *American Mineralogist*, **57**, 1524–1527.

De Waal, S.A. (1978) The nickel deposit at Bon Accord, Barberton, South Africa – A proposed paleometeorite. Pp. 87–98 in: *Mineralisation in metamorphic terranes* (W.J. Verwoerd, editor). Special Publication, Geological Society of South Africa, Johannesburg, South Africa.

De Waal, S.A. (1979) The metamorphism of the Bon Accord nickel deposit by the Nelspruit granite. *Transactions of the Geological Society of South Africa*, **82**, 335–342.

De Waal, S.A. and Calk, L.C. (1973) Nickel minerals from Barberton, South Africa: VI: Liebenbergite, a nickel olivine. *American Mineralogist*, **58**, 733–735.

De Wit, M.J., Hart, R.A. and Hart, R.J. (1987) The Jamestown ophiolite complex, Barberton Mountain Land: A composite section through 3.5 Ga simatic lithosphere. *Journal of African Earth Sciences*, **6**, 681–730.

https://doi.org/10.1180/minmag.2015.079.7.07 Published online by Cambridge University Press

Helmy, H.M., Ballhaus, C., Fonseca, R.O.C., Wirth, R., Nagel, T. and Tredoux, M. (2013) Noble metal nanoclusters and nanophases precede mineral formation in magmatic sulphide melts. *Nature Communication* **4**, 2405, http://dx.doi:10.1038/ncomms3405

O'Driscoll, B., Clay, P.L., Lenaz, D., Cawthorn, R.G., Adetunji, J. and Kronz, A. (2014) Trevorite: Ni-rich spinel formed by metasomatism and desulphurisation processes at Bon Accord, South Africa? *Mineralogical Magazine*, **78**, 145–163.

Okamoto, H. (2009) Ni-Sb (Nickel-Antimony). *Journal of Phase Equilibria and Diffusion*, **30**, 301–302.

Partridge, F.C. (1944) Trevorite and a suggested new nickel-bearing silicate from Bon Accord, Sheba Siding, Barberton district. *Transactions of the Geological Society of South Africa*, **46**, 119–126.

Raghavan, V. (2004) Fe-Ni-Sb (Iron-Nickel-Antimony). *Journal of Phase Equilibria and Diffusion*, **25**, 553.

Tredoux, M., de Wit, M.J., Hart, R.J., Armstrong, R.A., Lindsay, N.M. and Sellschop, J.P.F. (1989) Platinum group elements in a 3.5 Ga nickel-iron occurrence, Possible evidence of a deep mantle origin. *Journal of Geophysical Research*, **94**(B1), 795–813.

Tredoux, M., Roelofse, F. and Shukolyukov, A. (2014) A Cr isotopic study of the Bon Accord NiO body, Barberton greenstone belt, South Africa. *Chemical Geology*, **390**, 182–190.

Trevor, T.G. (1920) Nickel: Notes on the occurrence in the Barberton district. *South African Journal of Industry*, **3**, 532–533.

Walker, T.L. (1923) Trevorite a distinct mineral species. *University of Toronto Studies*, **16**, 53.

Wildau, A. (2012) An investigation of microscopic phases in the Bon Accord Ni-oxide body, Barberton region, South Africa. Unpublished M.Sc. dissertation. University of the Free State, Bloemfontein, South Africa.

Zaccarini, F., Tredoux, M., Miller, D.E., Garuti, G., Aiglsperger, T. and Proenza, J.A. (2014) The occurrence of platinum-group and gold minerals in the Bon Accord Ni-oxide body, South Africa. *American Mineralogist*, **99**, 1774–1782.